Theoretical Studies of the Reaction of Hydroxyl Radical with Methyl Acetate

Lei Yang, Jing-yao Liu,* and Ze-sheng Li*

Institute of Theoretical Chemistry, State Key Laboratory of Theoretical and Computational Chemistry, Jilin University, Changchun 130023, People's Republic of China

Received: February 1, 2008; Revised Manuscript Received: March 28, 2008

The mechanisms and the kinetics of the OH (OD) radicals with methyl acetate $CH_3C(O)OCH_3$ are investigated theoretically. The dual-level direct dynamics method is employed in the calculation of the rate constants. The optimized geometries and frequencies and the gradients of the stationary points are calculated at the MP2/6-311G(d,p) level. The energetic information of potential energy surfaces is further refined by the multicoefficient correlation method based on QCISD (MC-QCISD) using the MP2/6-311G(d,p) geometries. Four channels are found for the title reaction. The calculated results reveal that there exists an attractive well (reactant complex) in each entrance H-abstraction channel, that is, the H-abstraction reaction makes a stepwise mechanism. The rate constants are calculated by the canonical variational transition-state theory (CVT) with the interpolated single-point energies (ISPE) approach in the temperature range of 200−1200 K. The small-curvature tunneling effect (SCT) approximation is used to evaluate the transmission coefficient. The calculated rate constants are in good agreement with the experimental ones in the measured temperature range. It is shown that the "out-of-plane hydrogen abstraction" from the methoxy end is the dominant channel at the lower temperatures, and the other two H-abstraction channels should be taken into account with the temperatures increasing. The kinetic isotope effects (KIEs) for the three H-abstraction channels and the total reaction are "inverse", and these theoretically calculated KIEs as a function of temperature are expected to be useful for the future laboratory investigation.

Introduction

Volatile organic compounds (VOCs) are emitted to the atmosphere through their use in industry and by biogenic sources. As one important class of VOCs, esters have been widely used in industry, particularly as a solvent and in the manufacture of perfumes and flavoring. They can be produced naturally through vegetation and be emitted directly into the atmosphere, and the degradation of some oxygenated compounds is also a source of esters. For example, methyl acetate can be produced from methyl tert-butyl ether (MTBE)[1,2] and tert-amyl ether (TAME).[3] As it is well known, the atmospheric oxidation processes of VOCs initiated by OH may contribute to the photochemical formation of ozone and other components of photochemical smog found in urban areas. However, it was found that methyl acetate shows a significantly lower photochemical ozone creation potential (POCP) and would appear to offer significant environmental advantages as a substitute solvent.[4] Thus, methyl acetate has considerable potential for substitution in industry. Prior to its large-scale industrial use, it is very necessary to evaluate the atmosphere lifetime and the environmental impact of methyl acetate.

Despite the importance of methyl acetate, its atmospheric oxidation mechanism has received relatively little attention. The oxidation of esters is largely initiated by the reaction with OH radicals, while photolysis and reactions with other oxidants (such as reactions with O_3 and NO_3 radicals) may play a less important role in their atmospheric degradation.[5] Therefore, methyl acetate may be released into the atmosphere during its industrial use and is degraded in the troposphere almost exclusively via its reaction with OH radical. The rate constants for the reaction $CH_3C(O)OCH_3 + OH \rightarrow$ products were measured using the pulsed laser photolysis−laser-induced fluorescence technique over the temperature range of 243−372 K by Boudali et al.,[6] and the Arrhenius expression was fitted as $k = (0.53 \pm 0.09) \times 10^{-12} \exp[-(128 \pm 102)/T]$ cm^3 molecule^{-1} s^{-1}. Also, Wallington et al.[7] gave a rate constant expression over the range of 240−440 K as $k = (8.3 \pm 3.5) \times 10^{-13} \exp[-(260 \pm 150)/T]$ cm^3 molecule^{-1} s^{-1}. It is seen that the two experiments are within their error bars for both the preexponential factor and for the activation energy. In addition, Smith et al.[8] determined the rate constants of this reaction at 298 K with a value of $(3.85 \pm 0.349) \times 10^{-13}$ cm^3 molecule^{-1} s^{-1}, in reasonable agreement with the values obtained by the above two groups,[6,7] while they are about 2 times larger than that obtained by Campbell et al.[9] Since there are such discrepancies between them, it is very desirable to perform a theoretical investigation for better understanding. Unfortunately, to the best of our knowledge, little theoretical attention has been paid to the title reaction on the detailed reaction mechanisms and the information of branching ratios.

In the present work, a dual-level (X//Y) direct dynamics method[10–12] is employed to investigate the title reaction. First, high-level ab initio electronic structure calculations are performed to find stationary points along the reaction path (reactants, products, intermediate complexes, and transition states), and the MC-QCISD method[13] is used to calculate the high-level single-point energies. It is well known that the reactions of OH with oxygenated compounds may proceed via the formation of complexes that involve one or two hydrogen bonds. As Smith and Ravishankara[14] said, these attractive wells in the entrance channel of a potential energy surface can influence the dynamics and, hence, the course of the reaction.

* To whom correspondence should be addressed. Fax: +86-431-88498026. E-mail: ljy121@mail.jlu.edu.cn. (J.-y.L.); zeshengli@mail.jlu.edu.cn (Z.-s.L.).

10.1021/jp800986d CCC: $40.75
Published on Web 06/20/2008

In the present study, the reactant and product complexes are also found at the entrance and exit of each channel. Subsequently, the rate constants for the title reaction are calculated over a wide temperature range of 200−1200 K using the variational transition-state theory (VTST)[15–17] with interpolated single-point energies (ISPE).[18] The total rate constants and the product branching ratios are obtained. Furthermore, the kinetic isotope effects are calculated in order to provide useful information for the future experiment. Finally, the comparison between theoretical and experimental rate constants is discussed.

Computational Methods

All of the electronic structure calculations were performed with the Gaussian 03 programs. The geometries and frequencies of all of the stationary points were obtained by using restricted and unrestricted second-order Møller−Plesset perturbation theory[19] with the 6-311G(d,p) basis set. At the same level, the minimum-energy path (MEP) was obtained by intrinsic reaction coordinate (IRC) theory to confirm that the transition state really connects with reactants and products as expected. Also, the energy derivatives including gradients and Hessians at geometries along the MEP were obtained to calculate the curvature of the reaction path and the generalized vibrational frequencies along the reaction path at the same level. The energies of all the stationary points were improved by single-point energy calculations using the multicoefficient correlation method based on quadratic configuration interaction with single and double excitations (MC-QCISD),[13] which has been identified as a very efficient method for the open-shell systems. The energy profiles were corrected with the interpolated single-point energies (ISPE) method.[18] For this method, as mentioned by Truhlar et al.,[18] four single-point calculations are important to correct the lower-level reaction path; two points are close to the 300 K turning points and are useful primarily to estimate the width of the barrier, and two other points are close to the lower-level saddle point and are useful primarily to locate the dual-level saddle point. Therefore, these four single-point energies are chosen for the spline fit in the present work.

Dynamic calculations of the reaction were performed using the Polyrate 9.3 program.[20] Canonical variational transition-state theory (CVT)[21] with the small-curvature tunneling (SCT)[22,23] corrections was applied to evaluate the theoretical rate constants. The CVT rate constant for temperature T is expressed as

$$k^{\mathrm{CVT}}(T,s) = \min k^{\mathrm{GT}}(T,s) \quad (1)$$

$$k^{\mathrm{GT}}(T,s) = \kappa \frac{\sigma k_{\mathrm{B}} T}{h} \frac{Q^{\mathrm{GT}(T,s)}}{\phi^{\mathrm{R}}(T)} \mathrm{e}^{-V_{\mathrm{MEP}}(s)/k_{\mathrm{B}}T} \quad (2)$$

where $k^{\mathrm{GT}}(T,s)$ is the rate constant in generalized transition-state theory at the dividing surface s, with σ being the symmetry factor accounting for the possibility of more than one symmetry-related reaction path, k_{B} is the Boltzmann's constant, h is the Planck's constant, $\phi^{\mathrm{R}}(T)$ is the reactant partition function per unit volume (excluding symmetry numbers for rotation), κ is the tunneling factor, and $Q^{\mathrm{GT}}(T,s)$ is the partition function of a generalized transition state at s with a local zero of energy at $V_{\mathrm{MEP}}(s)$ and with all rotational symmetry numbers set to unity. The separable translational, vibrational, rotational, and electronic motion assumption was used to evaluate the partition functions. The rotational and translation partition functions were calculated classically. Most of the vibrational modes were treated as quantum mechanical separable harmonic oscillators, while the two low-frequency modes which correspond to hindered rotations were treated as hindered rotors. The hindered rotor approximation of Truhlar and Chuang[24,25] was used for calculating the partition function of them. The $^2\Pi_{3/2}$ and $^2\Pi_{1/2}$ excited states of OH, with a 140 cm^{-1} splitting due to spin−orbit coupling, were included in the calculation of the reactant electronic partition functions.

Results and Disscussion

Stationary Points. Our calculations indicate that the reactant $CH_3C(O)OCH_3$ has C_s symmetry, and thus, two channels are found for H-abstraction from the methoxy end, namely, "out-of-plane hydrogen abstraction" (channel R1a) and "in-plane hydrogen abstraction" (channel R1b). However, three hydrogens in the $-C(O)CH_3$ group are equivalent, and only one channel R2 is found for H-abstraction from the $-CH_3$ group of the acetyl end. Moreover, the OH radical can also attack the carbon atom in the −C(O) - group and produce $CH_3C(O)OH$ and CH_3O (R3). Therefore, four channels are feasible for the $CH_3C(O)OCH_3$ + OH reaction.

$$CH_3C(O)OCH_3 + OH \rightarrow CH_2C(O)OCH_3 + H_2O \quad \text{(R1a, R1b)}$$

$$CH_3C(O)OCH_3 + OH \rightarrow CH_3C(O)OCH_2 + H_2O \quad \text{(R2)}$$

$$CH_3C(O)OCH_3 + OH \rightarrow CH_3C(O)OH + CH_3O \quad \text{(R3)}$$

For the three H-abstraction channels, the reactant and product complexes are located at the entrance and exit of the reactions, indicating that the three H-abstraction channels may proceed via an indirect mechanism. However, for channel R3, no complexes are located. Figure 1 presents the structural parameters of all of the reactants, products, complexes, and transition states calculated at the MP2/6-311G(d,p) level along with the available experimental data of OH,[26,27] H_2O,[27] CH_3COOH,[28] and CH_3O.[29] As shown in Figure 1, the optimized parameters are in good agreement with the experimental values (given in the parentheses). The reactant complex CR1a is stabilized by two hydrogen bonds; one is the attractive interaction between the hydrogen atom in the OH radical and the oxygen atom in the carbonyl group, with the distance of the O···H bond as $d_{\mathrm{O}\cdots\mathrm{H}}$ = 1.94 Å, and the other is maintained between the oxygen atom in the OH radical and the H in the $-OCH_3$ group, at a distance of $d_{\mathrm{O}\cdots\mathrm{H}}$ = 2.77 Å. The case is similar for reactant complex CR2. Also, a hydrogen bond is formed between the hydrogen atom in the OH radical or H_2O molecule and the oxygen atom in the carbonyl group −C(O)− or ether linkage −O− with the distance of the O···H bond being 1.95, 2.48, 2.08, and 1.99 Å for complexes CR1b, CP1a, CP1b, and CP2, respectively, while the other bond lengths in these hydrogen-bond complexes are very close to those of the reactants and products. With respect to the transition states TS1a, TS1b, and TS2, the breaking bond C−H is elongated by 10.1, 10.8, and 11.6% in comparison to the C−H equilibrium bond length of CH_3COOCH_3, respectively, and the forming O−H bond is 34.8, 33.1, and 31.8%, respectively, longer than the regular bond length of the isolated H_2O. The elongation of the forming bond (O−H) is greater than that of the breaking bond (C−H), which indicates that the three transition state are all reactant-like, and the reaction may proceed via "early" transition states for these exothermic reactions. This behavior is consistent with Hammond's postulate. Also, the elongation of the forming bond (18.7%) is greater than that of the breaking bond (10.7%) for TS3.

Table 1 lists the harmonic vibrational frequencies of all of the stationary points calculated at the MP2/6-311G(d,p) level along with the available experimental values of CH_3COOCH_3,[30]

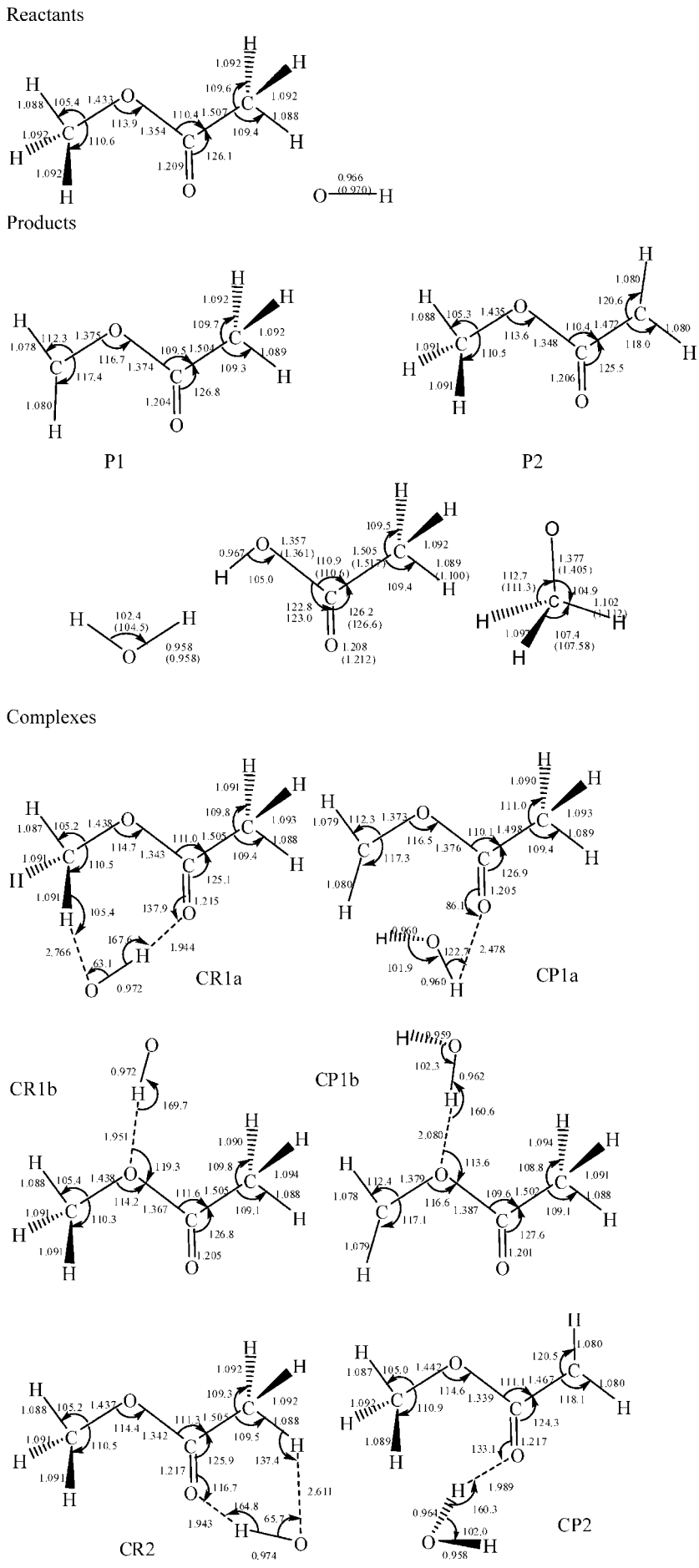

Figure 1. Part 1 of 2.

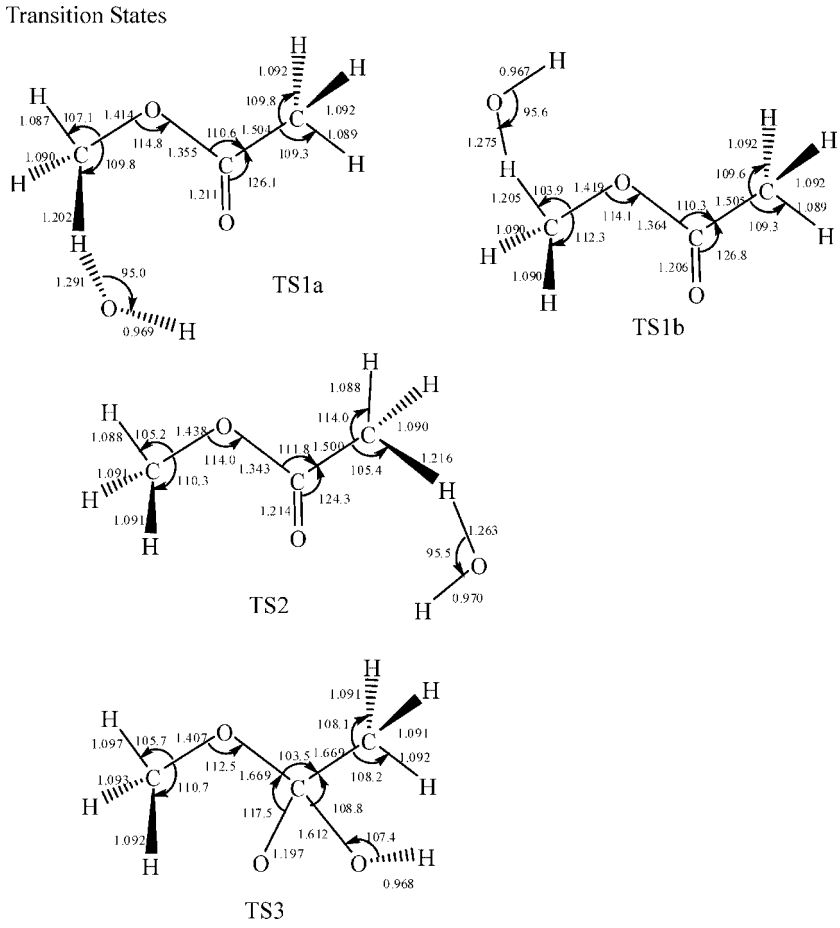

Figure 1. Part 2 of 2. Optimized geometries of reactants, products, complex, and transition states at the MP2/6-311G(d,p) level for the reaction $CH_3C(O)OCH_3$ + OH. The numbers in parentheses are the experimental values.[26–29] Bond lengths are in angstroms, and angles are in degrees.

CH_3COOH,[30] CH_3O,[29] OH,[26] and H_2O.[26,30] As seen from Table 1, the calculated frequencies are in reasonable agreement with the corresponding experimental results. All of the local minima including reactants, products, and complexes correspond to all real frequencies, and the transition state is confirmed by normal-mode analysis to have only one imaginary frequency corresponding to the stretching modes of the coupling between breaking and forming bonds. The imaginary frequencies of the transition states TS1a, TS1b, TS2, and TS3 are 2022i, 2051i, 2119i, and 1101i cm^{-1}, respectively. The reaction enthalpies $\Delta H_{298}°$ of the three reaction channels calculated at the two levels are listed in Table 2. The thermal corrections to the energy (TCE) at 298.15 K are included. As shown in Table 2, all of the reaction channels are exothermic, with the $\Delta H_{298}°$ values of −20.88, −20.88, −21.59, and −8.07 kcal/mol for R1a, R1b, R2, and R3, respectively, at the MC-QCISD//MP2 level.

An accurate knowledge of the enthalpy of formation ($\Delta H_{f,298}°$) of the species is required for a thorough understanding of the kinetics and mechanism of the reaction involved with them, particularly in the atmospheric modeling. Since there are no experimental or theoretical reports on the $\Delta H_{f,298}°$ of the species $CH_3C(O)OCH_2$ and $CH_2C(O)OCH_3$, to evaluate their $\Delta H_{f,298}°$ values, the following group-balanced isodesmic reactions[31] are used

$$CH_3C(O)OCH_2 + CH_4 \rightarrow CH_3C(O)CH_3 + CH_3 \quad \text{(R3a)}$$

$$CH_2C(O)OCH_3 + CH_4 \rightarrow CH_3C(O)CH_3 + CH_3 \quad \text{(R4)}$$

For $CH_3C(O)OCH_3$, there is one experimental report with the $\Delta H_{f,298}°$ value of −98.0 kcal/mol.[32] In order to verify the accuracy of above calculations, theoretical calculation is also carried out using the group-balanced isodesmic reactions

$$CH_3C(O)OCH_3 + CH_3CH_3 \rightarrow CH_3COCH_3 + CH_3OCH_3 \quad \text{(R5)}$$

The enthalpies of formation of the three molecules are evaluated by using the calculated reaction enthalpies of the isodesmic reactions (R3, R4, and R5) and the experimental $\Delta H_{f,298}°$ of the other species involved in the reactions (CH_3CH_3: −20.04 ± 0.07 kcal/mol;[33] CH_3COCH_3: −52.23 ± 0.14 kcal/mol,[34] CH_3OCH_3: −43.99 ± 0.12 kcal/mol;[35] CH_4: −17.89 kcal/mol;[36] $CH_3C(O)OCH_3$: −98.0 kcal/mol;[32] CH_3: 34.821 kcal/mol).[36] The computed $\Delta H_{f,298}°$ values at the MC-QCISD//MP2/6-311G(d,p) level are −97.51 ± 0.33, 49.65 ± 0.14, and −50.36 ± 0.14 kcal/mol for $CH_3C(O)OCH_3$, $CH_3C(O)OCH_3$, and $CH_3C(O)OCH_3$, respectively. Good agreement with the only one experimental value of methyl acetate (−98.0 kcal/mol)[32] infers that present theoretical predicts may be reliable. The error limits are obtained from the experimental errors in the components of the isodesmic reactions.

A schematic potential energy surface of the title reaction obtained at the MC-QCISD//MP2/6-311G(d,p) level considering the ZPE correction is plotted in Figure 2. The energy of the reactant is set to zero as a reference. As shown in Figure 2, the reaction of the OH radical with methyl acetate may proceed starting from attractive wells in the entrance valleys of the potential energy surfaces, that is, the formation of the hydrogen-bonded complexes CR1a, CR1b, and CR2. The stabilization

TABLE 1: Calculated Frequencies (cm^{-1}) of the Stationary Points at the MP2/6-311G(d,p) Level and the Experimental Values in Parentheses

species	frequencies (cm^{-1})
Rea	3225(3035),[a] 3225(3031),[a] 3188(3005),[a] 3187(2994),[a] 3102(2966),[a] 3098(2964),[a] 1828(1771),[a] 1528(1460),[a] 1510(1460),[a] 1501(1440),[a] 1498(1430),[a] 1494(1430),[a] 1415(1375),[a] 1294(1248),[a] 1228(1187),[a] 1202(1159),[a] 1104(1060),[a] 1074(1036),[a] 1002(980),[a] 876(844),[a] 654(639),[a] 604(607),[a] 429(429),[a] 295(303),[a] 184(187),[a] 162(136),[a] 28(110)[a]
OH	3854(3738)[b]
P1	3382, 3226, 3223, 3188, 3102, 1844, 1497, 1493, 1477, 1415, 1272, 1219, 1186, 1071, 1015, 845, 652, 601, 587, 439, 313, 259, 160, 61
P2	3367, 3231, 3229, 3194, 3102, 1978, 1527, 1508, 1507, 1474, 1334, 1230, 1202, 1100, 1012, 887, 758, 672, 552, 428, 298, 259, 188, 154
H_2O	4012(3756),[b] 3904(3657),[a] 1668(1595)[a]
CH_3COOH	3822(3583),[a] 3228(3051),[a] 3189(2996),[a] 3103(2944),[a] 1851(1788),[a] 1498(1430),[a] 1495(1430),[a] 1433(1382),[a] 1361(1264),[a] 1230(1182),[a] 1077(1048),[a] 1014(989),[a] 881(847),[a] 665(657),[a] 591(642),[a] 543(534),[a] 426, 75(93)[a]
CH_3O	3126(2840),[c] 3091(2758),[c] 3011(2758),[c] 1552(1412),[c] 1433(1047),[c] 1429(914),[c] 1142(914),[c] 991(651),[c] 830(651)[c]
CR1a	3762, 3234, 3227, 3200, 3190, 3104, 3103, 1813, 1535, 1522, 1506, 1498, 1493, 1420, 1318, 1233, 1211, 1101, 1077, 1007, 886, 657, 609, 523, 471, 436, 297, 248, 183, 157, 78, 53, 25
CP1a	3982, 3886, 3374, 3226, 3217, 3197, 3102, 1840, 1681, 1502, 1496, 1475, 1412, 1267, 1220, 1188, 1075, 1027, 841, 670, 658, 593, 443, 386, 320, 285, 269, 180, 165, 141, 129, 71, 61
CR1b	3762, 3228, 3228, 3199, 3192, 3104, 3102, 1841, 1528, 1509, 1507, 1501, 1493, 1421, 1267, 1229, 1202, 1100, 1077, 1010, 861, 655, 602, 593, 434, 397, 304, 188, 158, 147, 94, 59, 31
CP1b	3980, 3869, 3384, 3230, 3224, 3187, 3099, 1855, 1684, 1508, 1499, 1474, 1425, 1248, 1216, 1182, 1082, 1023, 825, 652, 602, 591, 523, 444, 324, 255, 226, 202, 168, 145, 104, 67, 36,
CR2	3721, 3232, 3231, 3195, 3189, 3104, 3102, 1801, 1526, 1510, 1504, 1503, 1496, 1423, 1325, 1229, 1201, 1106, 1081, 1008, 891, 663, 611, 608, 472, 440, 312, 189, 161, 151, 96, 85, 31
CP2	3971, 3837, 3368, 3241, 3232, 3207, 3107, 1848, 1702, 1536, 1525, 1513, 1478, 1360, 1240, 1200, 1095, 1018, 892, 750, 672, 582, 568, 434, 308, 280, 277, 200, 192, 159, 138, 96, 32
TS1a	3814, 3248, 3227, 3190, 3141, 3103, 1822, 1532, 1497, 1496, 1492, 1418, 1375, 1297, 1245, 1137, 1128, 1076, 1018, 945, 886, 763, 653, 605, 437, 410, 371, 285, 202, 143, 78, 35, 2022i
TS1b	3846, 3225, 3225, 3189, 3129, 3102, 1835, 1584, 1513, 1498, 1494, 1416, 1283, 1274, 1247, 1158, 1116, 1073, 1008, 941, 885, 728, 634, 595, 417, 290, 244, 180, 152, 100, 55, 33, 2051i
TS2	3799, 3245, 3233, 3196, 3152, 3103, 1804, 1565, 1525, 1510, 1502, 1469, 1331, 1249, 1228, 1201, 1118, 1064, 1037, 958, 889, 765, 651, 613, 401, 395, 320, 288, 197, 163, 130, 38, 2119i
TS3	3819, 3205, 3196, 3178, 3149, 3099, 3058, 1875, 1519, 1507, 1495, 1488, 1451, 1415, 1208, 1174, 1121, 1091, 1076, 994, 964, 629, 608, 542, 513, 502, 378, 357, 252, 210, 176, 164, 1101i

[a] From ref 30. [b] From ref 26. [c] From ref 29.

TABLE 2: Calculated Relative Enthalpies ($\Delta H298°$) and Potential Barriers (ΔE) (kcal/mol) Considering ZPE Correction

	$\Delta H298°$				ΔE			
method	R1a	R1b	R2	R3	R1a	R1b	R2	R3
MP2/6-311G(d,p)	−17.08	−17.08	−16.23	−7.28	4.34	7.60	6.39	31.74
MC-QCISD//MP2	−20.88	−20.88	−21.59	−8.07	1.66	4.90	4.33	8.35

energies are −4.24, −2.53, and −4.69 kcal/mol for CR1a, CR1b, and CR2, respectively. Then, each reactant complex undergoes a H-transfer process to form product complexes CP1a, CP1b, and CP2, which lie 1.98, 1.17, and 3.37 kcal/mol below the corresponding products P1 and P2, respectively. The potential barrier height for out-of-plane hydrogen abstraction from the methoxy end (R1a) (1.66 kcal/mol) is the lowest one. Therefore, channel R1a may be the major reaction pathway, and the other channels would be less favorable. With respect to the barrier heights of channels R1b and R2, the energy of TS1b (4.90 kcal/mol) is only 0.6 kcal/mol larger than that of TS2 (4.33 kcal/mol), and the former is more exothermic than the latter by about 0.5 kcal/mol. Thus, these two reaction channels may be competitive over the whole temperature range. This view will be verified by the rate constant calculation in the following section. In addition, the OH radical can also attack the carbon atom in the −C(O)− group and undergo a displacement process leading to $CH_3C(O)OH$ and CH_3O. However, the barrier height of this channel is 8.35 kcal/mol at the MC-QCISD//MP2 level, which is much larger than that of other channels. Thus, we only calculate the rate constants for the three H-abstraction channels in the following section.

Rate Constants Calculation. Dual-level dynamics calculations are carried out to study the kinetic nature of the title reaction. At the MP2/6-311G(d,p) level of theory, the MEP for each reaction channel is calculated by IRC theory, and the potential energy profile is further improved with the ISPE method at the MC-QCISD//MP2/6-311G(d,p) level. Note that for the title reaction, weak hydrogen-bonded complexes are formed at the entrance and exit channels; as a result, a stepwise mechanism occurs, that is

$$A + B \rightleftharpoons A\cdots B \quad \text{(step1)}$$

$$A\cdots B \rightarrow C\cdots D \quad \text{(step2)}$$

$$C\cdots D \rightarrow C + D \quad \text{(step3)}$$

In the present study, we assumed that the reaction occurs at the high-pressure limit, that is, the reactant complex undergoes collisional stabilization. This hypothesis and the approach have been detailed elsewhere and applied successfully to describe the reactions of the OH radical with several VOCs.[37–40] Here, for brevity, we just state, without details, that, on the basis of this assumption, the CVT rate constant expression for the present case is identical to eq 2, while the tunneling factor κ may become different with the existence of the prereactive complex. Under high-pressure-limit conditions, it is assumed that a thermal equilibrium distribution of the energy levels is maintained. Therefore, the energy levels from the bottom of the

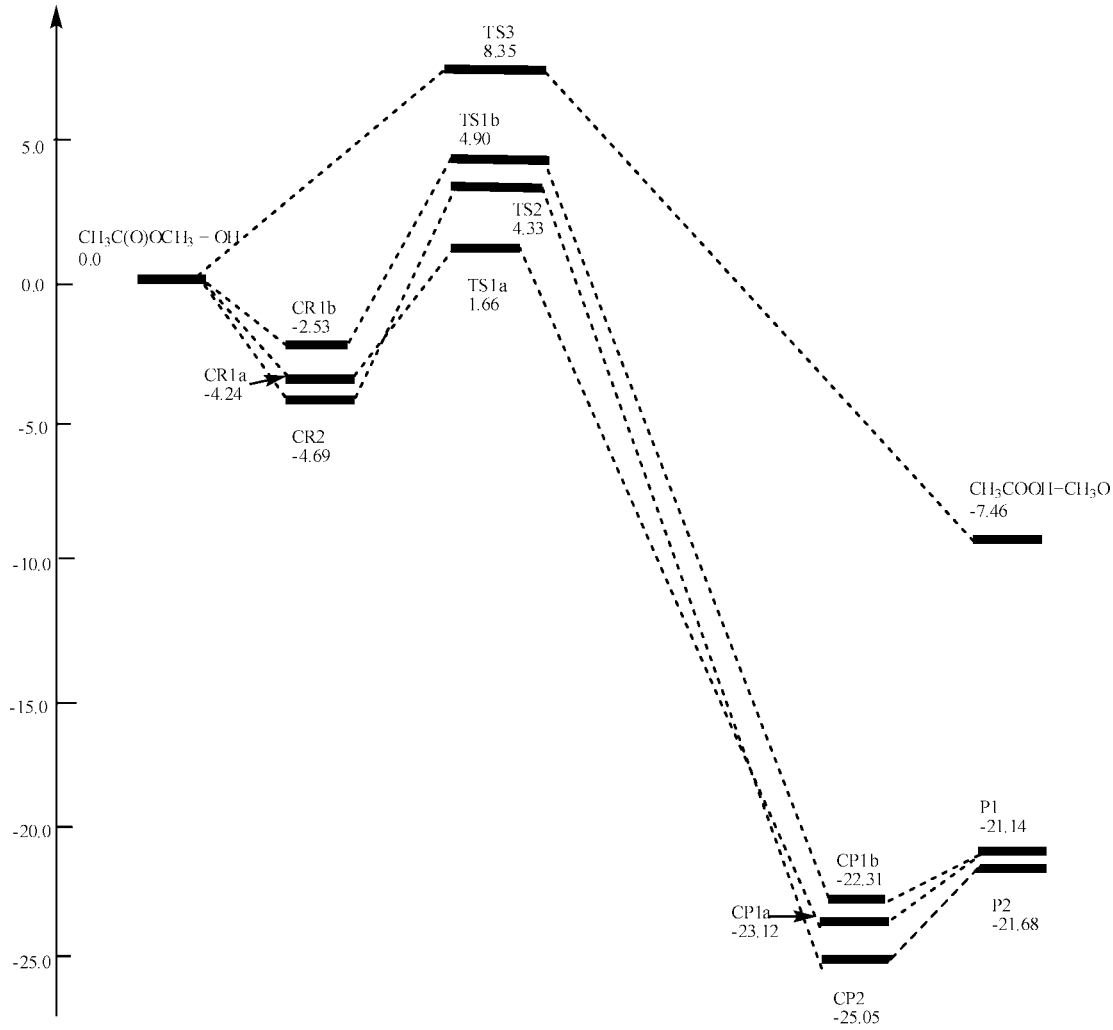

Figure 2. Schematic potential energy surface for the reaction $CH_3C(O)OCH_3 + OH$. Relative energies (in kcal/mol) are calculated at the MC-QCISD//MP2 level.

complex up to the barrier might contribute to the tunneling and lead to a corresponding increase in the tunneling factor in the present case.[41]

Figure 3a−c shows the plots of the classical potential energy curve (V_{MEP}), ground-state vibrationally adiabatic energy curve (V_a^G), and zero-point energy curve (ZPE) as functions of s (amu)$^{1/2}$ bohr at the MC-QCISD//MP2 level for channels R1a, R1b, and R2, where $V_a^G = V_{MEP} + ZPE$. It can be seen from these three figures that the ZPE is practically constants as s varies, with only a gentle drop near the saddle point, and the V_{MEP} and V_a^G curves are similar in shape. In Figure 3a−c, the maxima are also located at the same position, implying that the variational effect will be small or almost negligible for these three channels.

On the basis of the PES information obtained above, the rate constants are evaluated by the TST, CVT, and CVT with SCT correction over a wide temperature region from 200 to 1200 K. The plots of the TST, CVT, and CVT/SCT rate constants for channels R1a, R1b, and R2 are shown in Figure 4a−c. From Figure 4a−c, it can be found that the TST and CVT curves are almost the same, implying that the variational effect is small for channels R1a, R1b, and R2. For channels R1a and R2, the CVT/SCT values are about one or two orders of magnitude larger than the CVT values below 500 K, while they are asymptotic to the CVT ones at high temperature. Thus, the tunneling effect plays a significant role in the lower-temperature region for channels R1a and R2. The case is somewhat different for channel R1b. As seen from Figure 4b, the tunneling effect plays a role in the rate constant calculation at the low temperatures since the discrepancy of CVT/SCT and CVT values is moderate.

The total rate constants of the title reaction associated with the three pathways ($k = k_{1a} + k_{1b} + k_2$) and the available experimental values are described in Figure 5a, and for clarity, Figure 5b is provided to focus on only the comparison between theoretical and experimental results in the measured temperature range. In addition, the temperature dependence of the k_{1a}/k, k_{1b}/k, and k_2/k branching ratios is exhibited in Figure 6. As shown in Figure 6, the "out-of-plane hydrogen abstraction" from the methoxy end (channel R1a) is the dominant channel for the title reaction at the lower temperatures, and the other channels (R1b and R2) should be taken into account with increasing temperature. For example, the k_{1a}/k_1, k_{1b}/k_1, and k_2/k fractions are 97.9, 0.2, and 1.9% at 298 K and 49.4, 25.1, and 25.6% at 1000 K. From Figure 5a and b, we can see that our calculated rate constants show good agreement with the experimental data from refs 6–8 within a factor of 0.6−1.2 in the measured temperature range of 240−440 K, while the calculated rate constant at 292 K (3.41×10^{-13} cm^3 molecule^{-1} s^{-1}) slightly overestimates the experimental result measured by Campbell et al.[9] ((1.83 ± 0.5) $\times 10^{-13}$ cm^3 molecule^{-1} s^{-1}). On the basis of our calculated CVT/SCT values, the three-parameter expression (in units of

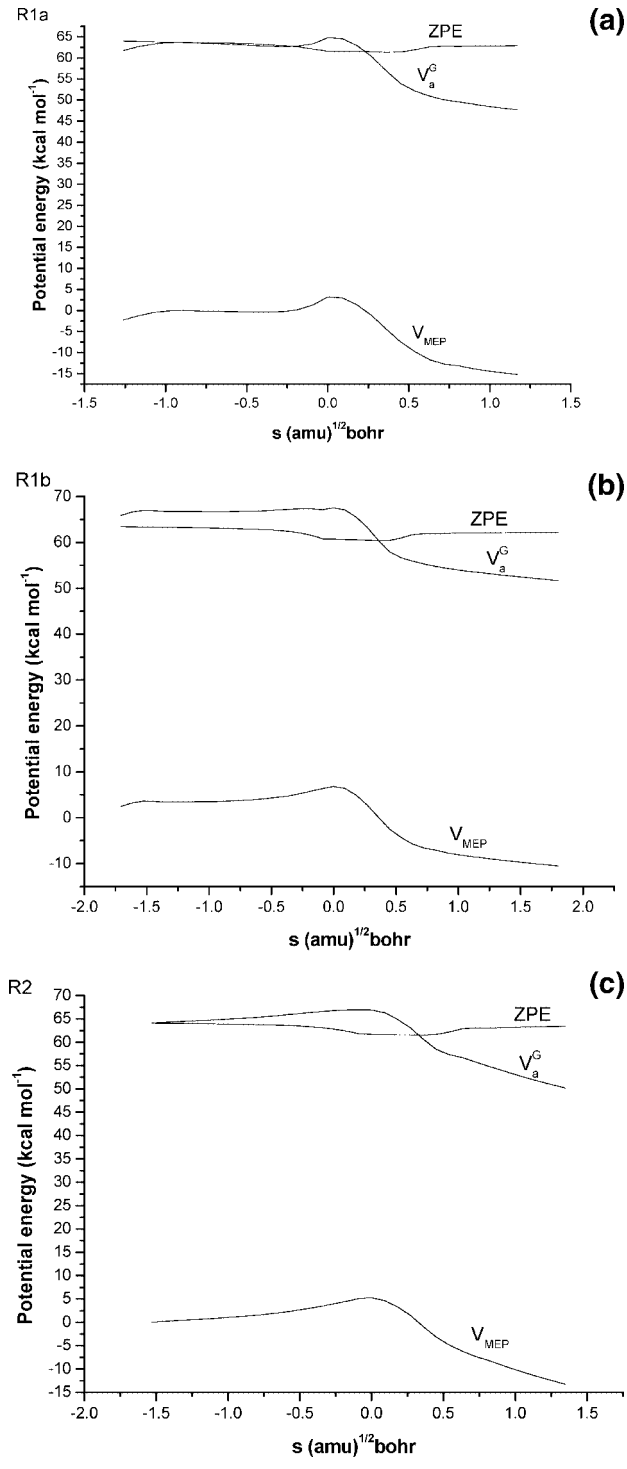

Figure 3. Classical potential energy curve (V_{MEP}), ground-state vibrationally adiabatic energy curve (V_a^G), and zero-point energy curve (ZPE) as functions of s (amu)$^{1/2}$ bohr at the MC-QCISD//MP2 level for reaction channels R1a (a), R1b (b), and R2 (c).

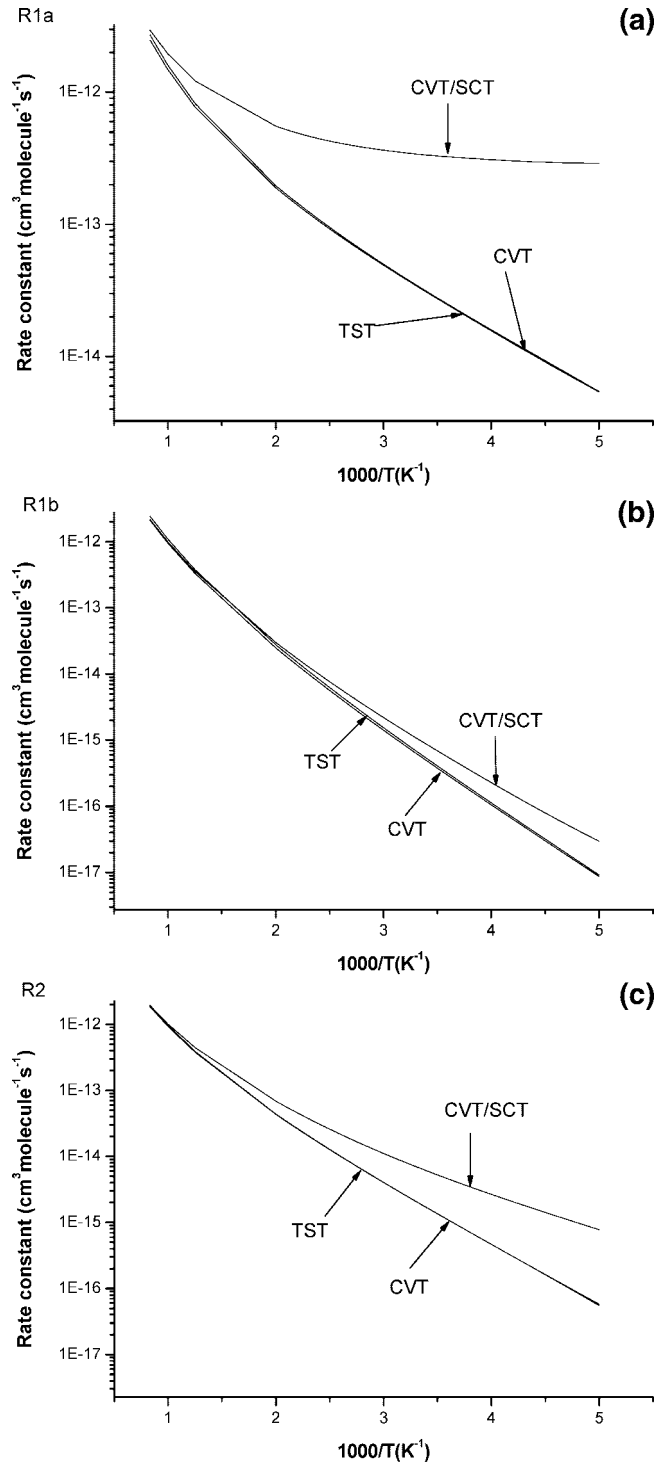

Figure 4. Computed TST, CVT, and CVT/SCT rate constants as a function of $10^3/T$ for the reaction channels R1a (a), R1b (b), and R2 (c).

cm^3 molecule^{-1} s^{-1}) is fitted as follows: $k_{1a} = 1.80 \times 10^{-20} T^{2.59} \exp(582/T)$; $k_{1b} = 2.87 \times 10^{-21} T^{3.04} \exp(-1381/T)$; $k_2 = 8.16 \times 10^{-22} T^{3.11} \exp(-542/T)$; $k = 8.76 \times 10^{-24} T^{3.75} \exp(887/T)$.

Kinetic Isotope Effects (KIEs). Figure 7 describes the OH/OD KIE against $1000/T$ (K^{-1}) for each channel (R1a, R1b, R2) and the total reaction R within the temperature range of 200−1200 K, in which the OH/OD KIE is defined as the ratio of the OH and OD reaction rate constant. It can be seen that the KIEs are within 0.8−1.0, 0.6−0.9, 0.7−1.0, and 0.8−1.0, respectively, for individual channels R1a, R1b, R2, and the total reaction and increases with increasing temperature. For each reaction, deuteration slightly enhances the rate coefficient, that is, the KIEs are "inverse" ($k_H/k_D < 1$). These inverse isotope effects have also been observed for many other reactions.[42–45] The theoretical rate constants of the $CH_3C(O)OCH_3$ + OD from CVT/SCT values within 200−1200 K are fitted by the three-parameter Arrhenius expression (in units of cm^3 molecule^{-1} s^{-1}): $k_{1a}' = 6.12 \times 10^{-21} T^{2.73} \exp(694/T)$; $k_{1b}' = 1.51 \times 10^{-21} T^{3.13} \exp(-1259/T)$; $k_2' = 2.31 \times 10^{-22} T^{3.27} \exp(-368/T)$; $k' = 2.38 \times 10^{-24} T^{3.93} \exp(1005/T)$. Since there is no corresponding

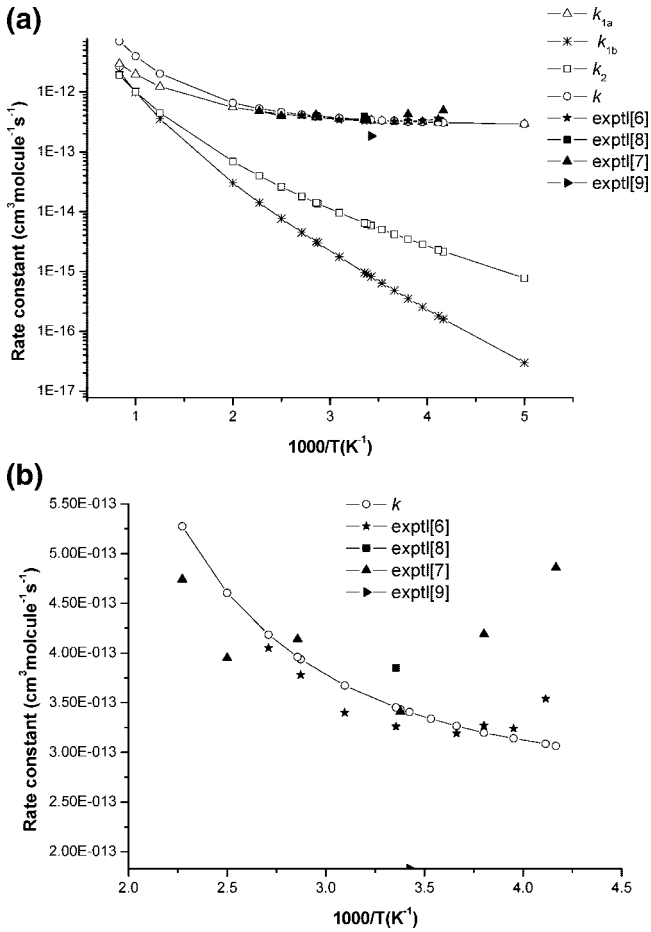

Figure 5. (a) Calculated rate constants k_{1a}, k_{1b}, and k_2 for the individual channels R1a, R1b, and R2, respectively, and the total rate constants k are obtained at the MC-QCISD//MP2 level along with the experimental values[6–9] as a function of $10^3/T$ in the temperature range of 200−1200 K. (b) Comparison of total rate constants k obtained at the MC-QCISD//MP2 level and the experimental values[6–9] in the measured temperature range of 240−440 K.

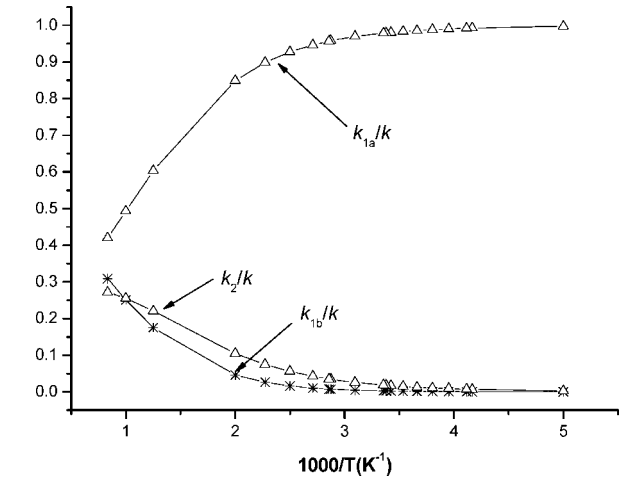

Figure 6. Calculated branching ratio for the $CH_3C(O)OCH_3$ + OH reaction as a function of $10^3/T$ at the MC-QCISD//MP2 level.

experimental value available, it is expected that our theoretical prediction can provide useful information for future study.

Conclusion

In this paper, a systematic investigation on the reaction $CH_3C(O)OCH_3$ with OH(OD) is performed. A dual-level dynamics method is employed to study the hydrogen-abstraction reaction mechanism. The potential energy surface information is obtained at the MP2/6-311G(d,p) level, and the energetic information is calculated by the MC-QCISD method. Three H-abstraction channels and one displacement process are identified. There exist the complexes with energies lower than the corresponding reactants or products for each H-abstraction reaction channel. The rate constants calculated by CVT with SCT correction are very consistent with the available experimental values. For channels R1a, R1b, and R2, the variational effect is very small over the whole temperature range, and the SCT correction plays a role at the lower temperatures. The calculated branching ratios show that the "out-of-plane hydrogen abstraction" from the methoxy end is the primary channel at the lower temperatures, while at the higher temperatures, the contribution of all of the H-abstraction reaction channels should be taken into account. The KIEs for three channels and the total reaction are all "inverse" and increase with increasing temperature. The three-parameter expression (in units of cm^3 molecule^{-1} s^{-1}) for the OH + $CH_3C(O)OCH_3$ and OD + $CH_3C(O)OCH_3$ reactions in the temperature range of 200−1200 K is fitted as follows: $k = 8.76\times 10^{-24}T^{3.75}\exp(887/T)$; $k' = 2.38\times 10^{-24}T^{3.93}\exp(1005/T)$.

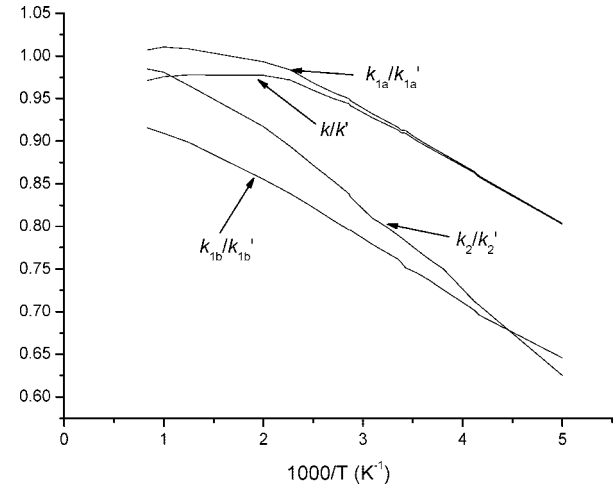

Figure 7. Plot of the calculated ratios k_{1a}/k_{1a}', k_{1b}/k_{1b}', k_2/k_2', and k/k' versus $1000/T$ in the temperature range of 200−1200 K.

TABLE 3: Enthalpies of Formation ($\Delta H_{f,298}°$) (kcal/mol) for the Species $CH_3C(O)OCH_3$, $CH_3C(O)OCH_2$, and $CH_2C(O)OCH_3$ at the MC-QCISD//MP/6-311G(d,p) Level, along with the Available Experimental Value (in parentheses)

	$CH_3C(O)OCH_3$	$CH_3C(O)OCH_2$	$CH_2C(O)OCH_3$
MC-QCISD//MP2	-97.5 ± 0.33 (-98.0)[a]	-49.65 ± 0.14	-50.36 ± 0.14

[a] From ref 32.

Acknowledgment. We thank Professor Donald G. Truhlar for providing the POLYRATE 9.3 program. This work is supported by the National Natural Science Foundation of China (20333050, 20073014, 20303007), Program for New Century Excellent Talents in University (NCET), Doctor Foundation by the Ministry of Education Foundation for University Key Teacher by the Ministry of Education, and Key Subject of Science and Technology by the Ministry of Education of China, and the Innovation Foundation by Jilin University.

References and Notes

(1) Tuazon, E. C.; Carter, W. P. L.; Aschmann, S. M.; Atkinson, R. *Int. J. Chem. Kinet.* **1991**, *23*, 1003.

(2) Smith, D. F.; Kleindienst, T. E.; Hudgens, E. E.; McIver, C. D.; Bufalini, J. J. *Int. J. Chem. Kinet.* **1991**, *23*, 907.

(3) Smith, D. F.; McIver, C. D.; Kleindienst, T. E. *Int. J. Chem. Kinet.* **1995**, *27*, 453.

(4) Derwent, R. G.; Jenkin, M. E.; Saunders, S. M. *Atmos. Environ.* **1996**, *30*, 181.

(5) Mellouki, A.; Bras, G. L.; Sidebottom, H. *Chem. Rev.* **2003**, *103*, 5077.

(6) Boudali, A. E.; Galve, S. L.; Bras, G. L.; Mellouki, A. *J. Phys. Chem.* **1996**, *100*, 12364.

(7) Wallington, T. J.; Dagaut, P.; Liu, R.; Kurylo, M. J. *Int. J. Chem. Kinet.* **1988**, *20*, 177.

(8) Smith, D. F.; McIver, C. D.; Kleindienst, T. E. *Int. J. Chem. Kinet.* **1995**, *27*, 453.

(9) Campbell, I. M.; Parkison, P. E. *Chem. Phys. Lett.* **1978**, *53*, 385.

(10) Truhlar, D. G. In *The Reaction Path in Chemistry: Current Approaches and Perspectives*; Heidrich, D., Ed.; Kluwer: Dordrecht, The Netherlands, *1995*; p 229.

(11) Truhlar, D. G.; Garrett, B. C.; Klippenstein, S. J. *J. Phys. Chem.* **1996**, *100*, 12771.

(12) Hu, W. P.; Truhlar, D. G. *J. Am. Chem. Soc.* **1996**, *118*, 860.

(13) Fast, P. L.; Truhlar, D. G. *J. Phys. Chem. A* **2000**, *104*, 6111.

(14) Smith, L. W. M.; Ravishankara, A. R. *J. Phys. Chem. A* **2002**, *106*, 4798.

(15) Truhlar, D. G.; Garrett, B. C. *Acc. Chem. Res.* **1980**, *13*, 440.

(16) Truhlar, D. G., Isaacson, A. D., Garrett, B. C., Baer, M., Eds.; CRC Press: Boca Raton, FL, 1985; Vol. 65, p 1985.

(17) Truhlar, D. G.; Garrett, B. C. *Annu. Rev. Phys. Chem* **1984**, *35*, 159.

(18) Chuang, Y. Y.; Corchado, J. C.; Truhlar, D. G. *J. Phys. Chem. A* **1999**, *103*, 1140.

(19) Hehre, W. J.; Radom, L.; Schleyer, P. v. R.; Pople, J. A. *Ab Initio Molecular Orbital Theory*; Wiley: New York, 1986.

(20) Corchado, J. C.; Chuang, Y. Y.; Fast, P. L.; Hu, W. P.; Liu, Y. P.; Lynch, G. C.; Nguyen, K. A.; Jackels, C. F.; Ramos, A. F.; Ellingson, B. A.; Lynch, B. J.; Melissas, V. S.; Villa, J.; Rossi, I.; Coitino, E. L.; Pu, J.; Albu, T. V. *POLYRATE*, version 9.3.1; University of Minnesota: Minneapolis, MN, 2005.

(21) Garrett, B. C.; Truhlar, D. G. *J. Chem. Phys.* **1979**, *70*, 1593.

(22) Lu, D. H.; Truong, T. N.; Melissas, V. S.; Lynch, G. C.; Liu, Y. P.; Grarrett, B. C.; Steckler, R.; Issacson, A. D.; Rai, S. N.; Hancock, G. C.; Lauderdale, J. G.; Joseph, T.; Truhlar, D. G. *Comput. Phys. Commun.* **1992**, *71*, 235.

(23) Liu, Y. P.; Lynch, G. C.; Truong, T. N.; Lu, D. H.; Truhlar, D. G.; Garrett, B. C. *J. Am. Chem. Soc.* **1993**, *115*, 2408.

(24) Trhular, D. G. *J. Comput. Chem.* **1991**, *12*, 266.

(25) Chuang, Y. Y.; Truhlar, D. G. *J. Chem. Phys.* **2000**, *112*, 1221.

(26) Huber, K. P.; Herzberg, G. *Molecular Spectra and Molecular Structure. IV. Constants of Diatomic Molecules*; Van Nostrand Reinhold Co.: New York, 1979.

(27) Hoy, A. R.; Bunker, P. R. *J. Mol. Struct.* **1979**, *74*, 1.

(28) Hellwege, K. H., Hellwege, A. M., Eds. *Landolt-Bornstein: Group II: Atomic and Molecular Physics Volume 7: Structure Data of Free Polyatomic Molecules*; Springer-Verlag: Berlin, Germany, 1976.

(29) Jacox, M. E. *J. Phys. Chem. Ref. Data, Monograph 3*, **1994**.

(30) Shimanouchi, T. In *Tables of Molecular Vibrational Frequencies*, Consolidated Volume 1; NSRDS NBS-39.

(31) Good, D. A.; Francisco, J. S. *J. Phys. Chem. A* **1998**, *102*, 7143.

(32) Hall, H. K., Jr.; Baldt, J. H. *J. Am. Chem. Soc.* **1971**, *93*, 140.

(33) Pittam, D. A.; Pilcher, G. *J. Chem. Soc., Faraday Trans.* **1972**, *68*, 2224.

(34) Wiberg, K. B.; Crocker, L. S.; Morgan, K. M. *J. Am. Chem. Soc.* **1991**, *113*, 3447.

(35) Pilcher, G.; Pell, A. S.; Coleman, D. J. *Trans. Faraday Soc.* **1964**, *60*, 499.

(36) Chase, M. W., Jr. NIST-JANAF Themochemical Tables; Fourth Edition. *J. Phys. Chem. Ref. Data, Monograph 9* **1998**, 1–1951.

(37) Alvarez-Idaboy, J. R.; Mora-Diez, N.; Vivier-Bunge, A. *J. Am. Chem. Soc.* **2000**, *122*, 3715.

(38) Alvarez-Idaboy, J. R.; Mora-Diez, N.; Boyd, R. J.; Vivier-Bunge, A. *J. Am. Chem. Soc.* **2001**, *123*, 2018.

(39) Cruz-Torres, A.; Galano, A. *J. Phys. Chem. A* **2007**, *111*, 1523.

(40) Wang, Y.; Liu, J.-y.; Li, Z.-s. *J. Comput. Chem.* **2007**, *28*, 2517.

(41) Galano, A.; Alvarez-Idaboy, J. R.; Ruiz-Santoyo, M. E.; Vivier-Bunge, A. *J. Phys. Chem. A* **2005**, *109*, 169.

(42) Baeza-Romero, M. T.; Glowacki, D. R.; Blitz, M. A.; Heard, D. E.; Pilling, M. J.; Rickard, A. R.; Seakins, P. W. *Phys. Chem. Chem. Phys.* **2007**, *9*, 4114.

(43) Butkovskaya, N. I.; Pouvesle, N.; Kukui, A.; Mu, Y.; Bras, G. L. *J. Phys. Chem. A* **2006**, *110*, 6833.

(44) Jaramillo, V.; Smith, M. A. *J. Phys. Chem. A* **2001**, *105*, 5854.

(45) Butkovskaya, N. I.; Setser, D. W. *J. Phys. Chem. A* **1999**, *103*, 6921.

JP800986D